

BAROCLINIC WAVE TRANSITIONS, AUTUMN WEATHER PATTERNS, AND DUST STORMS IN THE NORTHERN HEMISPHERE OF MARS.

David Hinson^{1,2}, Huiqun Wang³, and Michael Smith⁴, ¹Carl Sagan Center, SETI Institute, Mountain View, CA 94043, USA (dhinson@seti.org), ²Department of Electrical Engineering, Stanford University, Stanford, CA 94305, USA, ³Atomic and Molecular Physics Division, Smithsonian Astrophysical Observatory, Cambridge, MA 02138, USA (hwang@cfa.harvard.edu), ⁴Laboratory for Extraterrestrial Physics, NASA Goddard Space Flight Center, Greenbelt, MD 20771, USA (michael.d.smith@nasa.gov).

Introduction. We are investigating several aspects of Martian meteorology through analysis and intercomparison of an assortment of observations. The data sets considered here include surface pressures measured by the Viking Landers (VL) [1, 2], wide-angle images acquired by the Mars Orbiter Camera (MOC) on Mars Global Surveyor (MGS) [3, 4], and atmospheric profiles obtained by MGS through two techniques: infrared sounding by the Thermal Emission Spectrometer (TES) [5] and Radio Science (RS) occultation experiments [6].

Our research has two main objectives. First, we are examining the behavior of baroclinic eddies in the northern hemisphere by applying essentially the same method of spectral analysis to the VL, TES, and RS data. The results are revealing key similarities and differences among the weather systems that appear in different Martian years. Second, we are also exploring the relationship between these baroclinic eddies and regional dust storms in the topographic basins of the northern hemisphere, identifying key factors that influence the timing and location of these events.

In assigning numbers to years we adopt the convention that Mars year 1 (MY 1) began on 11 April 1955.

Baroclinic wave transitions. Between late summer and early spring, an assortment of baroclinic waves appears at midlatitudes in the northern hemisphere and dominates the dynamics near the surface [e.g., 1, 7, 8, 9, 2, 10, 11, 12, 13, 14]. These eastward traveling waves comprise a coherent sequence of high and low pressure systems, and their periodicity in longitude allows distinct modes to be classified according to their zonal wave number (1–3) [e.g., 11, 12, 13, 14]. The amplitudes of the various modes are often anticorrelated — when one mode is strong the others are weak or absent. Once established, the dominant mode typically persists for 15–30 sols with a steady or slowly drifting frequency. The dynamics evolve through a sequence of baroclinic wave transitions in which the dominant mode fades rapidly and is superseded by another mode with a different zonal wave number and period. This type of behavior was first identified explicitly through analysis and numerical modeling of pressure measurements by Viking Lander 2 (VL2) [10]. The same phenomenon is apparent in RS measurements of both geopotential height and temperature [13, 14].

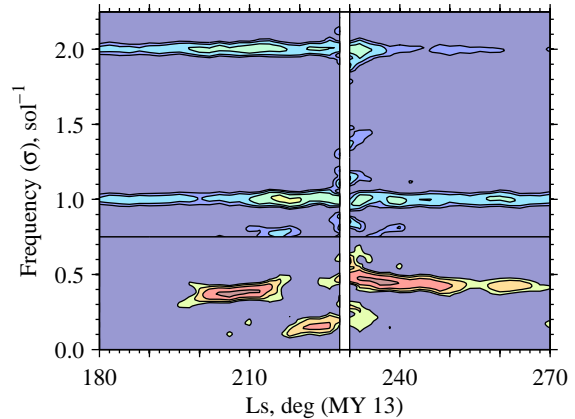


Figure 1: Spectrogram of surface pressure measured by VL2 (48°N, 134°E), showing the evolution of thermal tides and baroclinic eddies. Different contour levels are used in the upper and lower portions of the figure. The peak contour level corresponds to an amplitude of 1.2% for thermal tides ($\sigma > 0.75 \text{ sol}^{-1}$) and 3.0% for baroclinic eddies ($\sigma < 0.75 \text{ sol}^{-1}$). Each successive contour represents a doubling of power.

The VL pressure measurements have already received considerable attention [e.g., 1, 7, 8, 9, 15, 2, 10, 16]. We have two reasons for revisiting these data. First, we use a method of spectral analysis that facilitates comparisons with results derived from other instruments. Second, we present the results in a novel format that illustrates basic phenomena clearly and concisely.

We adopt a simple model to represent the time variations in surface pressure p recorded by VL2:

$$\hat{p} \equiv \bar{p}(L_s) + p'(t_u), \quad (1)$$

where L_s is the solar longitude and t_u is universal time. The first term \bar{p} is the gradual seasonal trend, while the second term p' represents the oscillations caused by traveling waves. The wave dynamics are represented using simple periodic basis functions:

$$p'(t_u) \equiv A \cos(2\pi\sigma t_u - \epsilon). \quad (2)$$

The wave model contains three free parameters: the amplitude A , the frequency σ , and the phase ϵ . We define the period $P \equiv \sigma^{-1}$.

Properties of the traveling waves are determined as follows. Within subsets of data spanning 8° of L_s (~ 15 sols), we solve for the seasonal trend \bar{p} by fitting a quadratic polynomial to samples of p versus L_s . We then search systematically for traveling waves by comparing the wave model with the detrended data, $p - \bar{p}$, obtaining least squares solutions for A and ϵ for a range of assumed values of σ .

We applied this method of analysis to data recorded by VL2 during autumn of its second year of operation (MY 13). Fig. 1 displays the results in the form of a spectrogram. There were no major planet-encircling dust storms during this interval, and there is only one significant gap in the data, near $L_s = 229^\circ$. These data contain the signature of several types of traveling waves [e.g., 9, 15, 2], which produce prominent spectral peaks in Fig. 1. An assortment of eastward traveling baroclinic eddies appears at low frequencies ($\sigma \leq 0.5 \text{ sol}^{-1}$), and these are accompanied by both diurnal tides ($\sigma = 1.0 \text{ sol}^{-1}$) and semidiurnal tides ($\sigma = 2.0 \text{ sol}^{-1}$).

The properties of these baroclinic eddies have been reported previously [e.g., 9, 17, 2, 10], but Fig. 1 is particularly effective at highlighting their key attributes: steady oscillations that persist for a span of 15–30 sols punctuated by abrupt transitions between modes with different properties. Three modes with distinctly different frequencies appear within this subset of observations: (1) $\sigma = 0.38 \text{ sol}^{-1}$ ($P = 2.6$ sols) at $L_s = 200\text{--}216^\circ$, (2) $\sigma = 0.15 \text{ sol}^{-1}$ ($P = 6.7$ sols) at $L_s = 218\text{--}226^\circ$, and (3) $\sigma = 0.45 \text{ sol}^{-1}$ ($P = 2.2$ sols) at $L_s = 228\text{--}250^\circ$. The first and third modes are the strongest, with peak amplitudes of about 3% in surface pressure.

According to numerical simulations [10], the baroclinic wave transitions are induced by dynamical jostling from the thermal tides. Fig. 1 provides circumstantial evidence in support of this conclusion. The amplitude of both the diurnal and semidiurnal tides varies significantly with time, possibly in response to dust lifting at some remote location [e.g., 2, 16]. In particular, the amplitude of the diurnal tide increases from $\sim 0.6\%$ at $L_s = 200\text{--}210^\circ$ to more than 1.2% at $L_s = 215\text{--}220^\circ$, with a peak value of $\sim 1.8\%$ near $L_s = 218^\circ$. The baroclinic wave transition at $L_s = 217^\circ$ may have been triggered by this transient intensification of the diurnal tide.

Weather patterns at midlatitudes in the northern hemisphere. We examined the weather at northern midlatitudes in several other Martian years by applying a similar method of spectral analysis to data acquired by the atmospheric sounders on MGS. These observations have significantly advanced our understanding of traveling waves on Mars. TES temperature profiles have yielded a comprehensive global characterization of the spatial structure and seasonal evolution of traveling waves [e.g., 11, 12, 18], while RS profiles of temperature

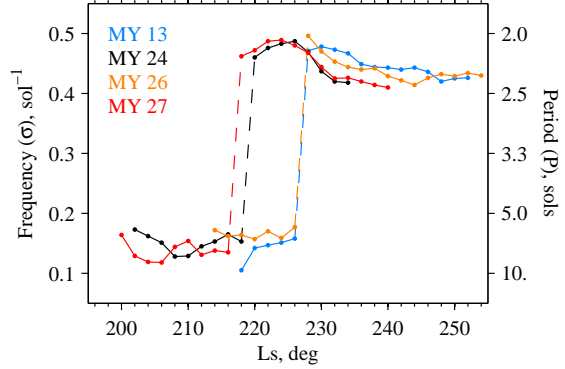


Figure 2: Evolution in frequency and period of the dominant baroclinic wave mode during midautumn of four Martian years. These results were derived through spectral analysis of VL2 measurements of p in MY 13 (blue), TES measurements of T at 610 Pa in MY 24 (black) and MY 26 (orange), and RS measurements of Z at 610 Pa in MY 27 (red). The dashed lines indicate baroclinic wave transitions where σ and P changed by a factor of ~ 3 .

and geopotential height have provided complementary results at selected seasons and latitudes [e.g., 19, 13, 14]. Nonetheless, much remains to be learned through further analysis of both data sets.

Atmospheric profiles retrieved from the TES and RS data are distributed in longitude, and Eqs. (1) and (2) must be modified accordingly. Within subsets of data at constant latitude and pressure, we characterize the zonal and temporal variations in temperature T by fitting a more general model to the measurements:

$$\hat{T} \equiv \bar{T}(L_s) + T'(\lambda, t_u). \quad (3)$$

The first term \bar{T} is the gradual seasonal trend, while the second term T' represents the oscillations caused by atmospheric waves, which now depend explicitly on east longitude λ :

$$T'(\lambda, t_u) \equiv A \cos(s\lambda - 2\pi\sigma t_u - \psi). \quad (4)$$

The zonal wave number s appears as a fourth free parameter in the wave model. We use expressions analogous to Eqs. (3) and (4) to model the zonal and temporal variations in geopotential height Z .

We systematically compared this model with subsets of TES and RS data spanning 8° of L_s , yielding least squares solutions for basic properties of the baroclinic eddies. We limit the present discussion to the 610-Pa pressure level, which is useful for characterizing the behavior of baroclinic eddies and their influence on the timing and location of regional dust storms [13, 14]. (The average surface pressure \bar{p} at VL2 increased from ~ 770 Pa to ~ 980 Pa during the interval shown in Fig. 1.)

Our method of data analysis facilitates direct comparisons among results derived from disparate instruments and different Martian years. For example, Fig. 2 characterizes a distinctive baroclinic wave transition that occurred in midautumn of MY 13, 24, 26, and 27. Mars experienced no major planet-encircling dust storms in these years. The results in MY 13 are from VL2 data at 48°N . The results in MY 24 and 26 are from TES data at latitudes of $60\text{--}65^\circ\text{N}$. The results in MY 27 are from RS data at 66°N .

Fig. 2 reveals intriguing similarities among the weather patterns in these four Martian years. A baroclinic wave transition occurs within this seasonal window in every year, and the properties of the baroclinic wave modes are remarkably similar. In both the TES and RS observations, the dominant wave mode initially has a zonal wave number $s = 1$ and a period P of ~ 7 sols. After the abrupt transition, the zonal wave number increases to $s = 3$ with a commensurate decrease in P to ~ 2.3 sols. The waves observed by VL2 exhibit similar values of P , and their zonal wave numbers are almost certainly the same as those observed by the atmospheric sounders on MGS. This is a striking example of the often repetitive nature of Martian weather from year to year.

The baroclinic wave transition occurs significantly earlier in MY 24 and 27 ($L_s = 218^\circ$) than in MY 13 and 26 ($L_s = 227^\circ$). The reason for this difference is not understood, but it has an important impact on the Martian dust cycle, as discussed in the next section.

There is a particularly close resemblance between the weather patterns that appear in the years with an early transition. The $s = 3$ baroclinic wave observed at $L_s = 220\text{--}234^\circ$ of MY 24 is virtually indistinguishable from its counterpart in MY 27. In both cases, the $s = 3$ mode achieves its peak amplitude at $L_s = 224^\circ$ as P approaches 2.0 sol^{-1} . After $L_s = 228^\circ$, the amplitude of the $s = 3$ mode decreases as P increases steadily to ~ 2.3 sols.

Dust storms. The MOC has provided extensive observations of a distinctive type of dust storm that occurs during autumn and winter in the major topographic basins of the northern hemisphere [4, 20, 12, 21, 18, 14]. These storms originate through lifting and advection of dust by baroclinic eddies at high northern latitudes. On some occasions these “frontal” storms spread southward as dust is entrained into the near-surface winds of the Hadley circulation, and the resulting “flushing” or “cross-equatorial” storm can progress from high northern latitudes into the tropics in a span of a few sols. The diurnally-varying, near-surface winds associated with thermal tides and topographic circulations appear to play an important role in the transition between the frontal and flushing stages of these dust storms [20, 22].

Sequences of flushing dust storms generally appear

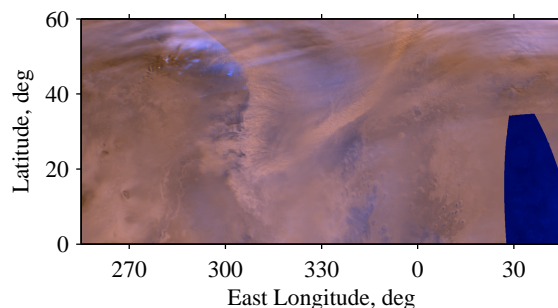


Figure 3: A regional dust storm observed by the MGS MOC in Acidalia Planitia at $L_s = 223.2^\circ$ of MY 24. The storm comprises two bands of dust that intersect at 305°E , 20°N (near VL1) in a distinctive “wishbone” configuration indicative of frontal activity [e.g., 24].

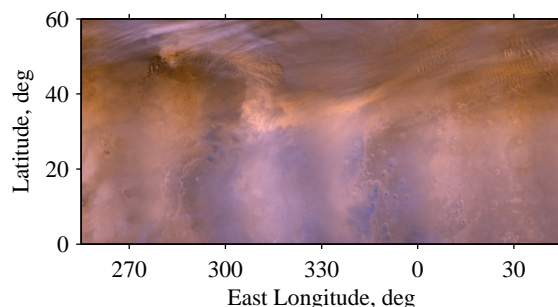


Figure 4: A regional dust storm observed by the MGS MOC in Acidalia Planitia at $L_s = 221.4^\circ$ of MY 27. This event occurred with a few sols of the anniversary of the dust storm in Fig. 3. Both storms were initiated by wave-3 baroclinic eddies.

within two distinct seasonal windows, one in midautumn and the other in midwinter, separated by a lull near winter solstice [18]. This pattern of dust-storm activity is correlated with seasonal variations in the amplitude and zonal wave number of the baroclinic eddies [12], which strongly modulate the intensity of meridional winds near the surface [13, 14]. Flushing dust storms occur most commonly in connection with wave-3 baroclinic eddies with periods of 2–3 sols. These conclusions are supported by several years of observations [12, 18, 14] as well as numerical simulations with a Mars General Circulation Model [20, 22, 23].

A series of vigorous frontal/flushing dust storms occurred in Acidalia Planitia during $L_s = 220\text{--}226^\circ$ of both MY 24 [4, 20] and MY 27 [14]. The onset of these storms is clearly a consequence of the baroclinic wave transition at $L_s = 218^\circ$ (Fig. 2), when the wave number of the dominant mode changes from $s = 1$ to $s = 3$ [14]. Figs. 3 and 4 show examples of the dust storms initiated by these baroclinic waves, revealing further similarities between the weather patterns in these two Martian years.

Dust storms of this intensity were absent from Acidalia in autumn of MY 26 [18], apparently because of the delayed arrival of the $s = 3$ baroclinic wave mode.

Acknowledgments. This research is supported by Grants NNX08AL24G (Hinson) and NNX07AR10G (Wang) of the NASA Mars Data Analysis Program.

References

- [1] J. A. Ryan, R. M. Henry, S. L. Hess, C. B. Leovy, J. E. Tillman, and C. Walcek. Mars meteorology - Three seasons at the surface. *Geophysical Research Letters*, 5:715–718, 1978. doi: 10.1029/GL005i008p00715.
- [2] R. W. Zurek, J. R. Barnes, R. M. Haberle, J. B. Pollack, J. E. Tillman, and C. B. Leovy. *Dynamics of the atmosphere of Mars*. In: Kieffer, H.H., Jakosky, B.M., Snyder, C.W., Matthews, M.S. (Eds.), *Mars*, pages 835–933. Univ. of Arizona Press, Tucson, 1992.
- [3] M. C. Malin and K. S. Edgett. Mars Global Surveyor Mars Orbiter Camera: Interplanetary cruise through primary mission. *Journal of Geophysical Research (Planets)*, 106:23429–23570, 2001. doi: 10.1029/2000JE001455.
- [4] B. A. Cantor, P. B. James, M. Caplinger, and M. J. Wolff. Martian dust storms: 1999 Mars Orbiter Camera observations. *Journal of Geophysical Research (Planets)*, 106(E10):23653–23688, 2001. doi: 10.1029/2000JE001310.
- [5] M. D. Smith. Interannual variability in TES atmospheric observations of Mars during 1999–2003. *Icarus*, 167: 148–165, 2004. doi: 10.1016/j.icarus.2003.09.010.
- [6] D. P. Hinson, R. A. Simpson, J. D. Twicken, G. L. Tyler, and F. M. Flasar. Initial results from radio occultation measurements with Mars Global Surveyor. *Journal of Geophysical Research (Planets)*, 104(E11):26997–27012, 1999. doi: 10.1029/1999JE001069.
- [7] C. B. Leovy. Martian meteorology. *Annual Reviews of Astronomy and Astrophysics*, 17:387–413, 1979. doi: 10.1146/annurev.aa.17.090179.002131.
- [8] J. R. Barnes. Time spectral analysis of midlatitude disturbances in the Martian atmosphere. *Journal of the Atmospheric Sciences*, 37:2002–2015, 1980. doi: 10.1175/1520-0469(1980)037.
- [9] J. R. Barnes. Midlatitude disturbances in the Martian atmosphere - A second Mars year. *Journal of the Atmospheric Sciences*, 38:225–234, 1981. doi: 10.1175/1520-0469(1981)038.
- [10] M. Collins, S. R. Lewis, P. L. Read, and F. Hourdin. Baroclinic Wave Transitions in the Martian Atmosphere. *Icarus*, 120:344–357, 1996. doi: 10.1006/icar.1996.0055.
- [11] D. Banfield, B. J. Conrath, P. J. Gierasch, R. J. Wilson, and M. D. Smith. Traveling waves in the martian atmosphere from MGS TES nadir data. *Icarus*, 170:365–403, 2004. doi: 10.1016/j.icarus.2004.03.015.
- [12] H. Wang, R. W. Zurek, and M. I. Richardson. Relationship between frontal dust storms and transient eddy activity in the northern hemisphere of Mars as observed by Mars Global Surveyor. *Journal of Geophysical Research (Planets)*, 110(E9):E07005, 2005. doi: 10.1029/2005JE002423.
- [13] D. P. Hinson. Radio occultation measurements of transient eddies in the northern hemisphere of Mars. *Journal of Geophysical Research (Planets)*, 111:E05002, 2006. doi: 10.1029/2005JE002612.
- [14] D. P. Hinson and H. Wang. Further observations of regional dust storms and baroclinic eddies in the northern hemisphere of Mars. *Icarus*, 206:290–305, 2010. doi: 10.1016/j.icarus.2009.08.019.
- [15] R. W. Zurek and C. B. Leovy. Thermal tides in the dusty martian atmosphere - A verification of theory. *Science*, 213:437–439, 1981.
- [16] R. J. Wilson and K. Hamilton. Comprehensive model simulation of thermal tides in the Martian atmosphere. *Journal of the Atmospheric Sciences*, 53:1290–1326, 1996.
- [17] J. A. Ryan and R. D. Sharman. Two major dust storms, one Mars year apart - Comparison from Viking data. *Journal of Geophysical Research*, 86:3247–3254, 1981. doi: 10.1029/JC086iC04p03247.
- [18] H. Wang. Dust storms originating in the northern hemisphere during the third mapping year of Mars Global Surveyor. *Icarus*, 189:325–343, 2007. doi: 10.1016/j.icarus.2007.01.014.
- [19] D. P. Hinson and R. J. Wilson. Transient eddies in the southern hemisphere of Mars. *Geophysical Research Letters*, 29(7):1154, 2002. doi: 10.1029/2001GL014103.
- [20] H. Wang, M. I. Richardson, R. J. Wilson, A. P. Ingersoll, A. D. Toigo, and R. W. Zurek. Cyclones, tides, and the origin of a cross-equatorial dust storm on Mars. *Geophysical Research Letters*, 30(9):1488, 2003. doi: 10.1029/2002GL016828.
- [21] B. A. Cantor. MOC observations of the 2001 Mars planet-encircling dust storm. *Icarus*, 186:60–96, 2007. doi: 10.1016/j.icarus.2006.08.019.
- [22] R. J. Wilson, D. Hinson, and M. D. Smith. GCM simulations of transient eddies and frontal systems in the martian atmosphere. In F. Forget, M. A. Lopez-Valverde, M. C. Desjean, J. P. Huot, F. Lefevre, S. Lebonnois, S. R. Lewis, E. Millour, P. L. Read, and R. J. Wilson, editors, *Mars Atmosphere Modelling and Observations*, pages 154–158, 2006.
- [23] S. Basu, J. Wilson, M. Richardson, and A. Ingersoll. Simulation of spontaneous and variable global dust storms with the GFDL Mars GCM. *Journal of Geophysical Research (Planets)*, 111:E09004, 2006. doi: 10.1029/2005JE002660.
- [24] J. L. Hollingsworth and M. A. Kahre. Extratropical cyclones, frontal waves, and Mars dust: Modeling and considerations. *Geophysical Research Letters*, 37:L22202, 2010. doi: 10.1029/2010GL044262.